



Published in final edited form as:

Science. 2013 November 15; 342(6160): 853–856. doi:10.1126/science.1243110.

Changes in Cytoplasmic Volume are Sufficient to Drive Spindle Scaling

James Hazel¹, Kaspars Krutkramelis², Paul Mooney¹, Miroslav Tomschik¹, Ken Gerow³, John Oakey², and J. C. Gatlin^{1,*}

¹Dept. of Molecular Biology, University of Wyoming, Laramie, WY 82071, USA

²Dept. of Chemical and Petroleum Engineering, University of Wyoming, Laramie, WY 82071, USA

³Dept. of Statistics, University of Wyoming, Laramie, WY 82071, USA

Abstract

The mitotic spindle must function in cell types that vary greatly in size, and its dimensions scale with the rapid, reductive cell divisions that accompany early stages of development. The mechanism responsible for this scaling is unclear, because uncoupling cell size from a developmental or cellular context has proven experimentally challenging. Here we combined microfluidic technology with *Xenopus* egg extracts to characterize spindle assembly within discrete, geometrically defined volumes of cytoplasm. Reductions in cytoplasmic volume, rather than developmental cues or changes in cell shape, were sufficient to recapitulate spindle scaling observed in *Xenopus* embryos. Thus, mechanisms extrinsic to the spindle, specifically a limiting pool of cytoplasmic component(s), play a major role in determining spindle size.

Organelles and other intracellular structures must scale with cell size in order to function properly. Maintenance of these dimensional relationships is challenged by the rapid and reductive cell divisions that characterize early embryogenesis in many organisms. The cellular machine that drives these divisions, the mitotic spindle, functions to segregate chromosomes in cells that vary greatly in size, while also adapting to rapid changes in cell size. The issue of scale is epitomized during *Xenopus* embryogenesis, where a rapid series of divisions reduces cell size 100-fold - from the 1.2 mm diameter fertilized egg to approximately 12 μm diameter cells in the adult frog (1). In large blastomeres, spindle length reaches an upper limit that is uncoupled from changes in cell size. As cell size decreases, however, a strong correlation emerges between spindle length and cell size (2). Although this scaling relationship has been characterized in vivo for several different organisms, little is known about the direct regulation of spindle size by cell size or the

*Correspondence to: jgatlin@uwyo.edu.

Supplementary Materials:
References (2, 12, 22, 26–31)
Materials and Methods
Supplementary Text
Figs. S1 to S3
Movies S1 to S5

underlying mechanism(s) (2–4). Spindle size may be directly dictated by the physical dimensions of a cell, perhaps through microtubule-mediated interaction with the cell cortex [i.e. boundary sensing; (5–7)]. Alternatively, cell size could constrain spindle length by providing a fixed and finite cytoplasmic volume and, therefore, a limiting pool of resources such as cytoplasmic spindle assembly or length-determining components [i.e. component limitation; (8, 9)]. Lastly, mechanisms intrinsic to the spindle could be actively tuned in response to systematic changes in cytoplasmic composition occurring during development [i.e. developmental cues; (10, 11)].

To elucidate the responsible scaling mechanism(s), we developed a microfluidic-based platform to confine spindle assembly in geometrically defined volumes of *Xenopus* egg extract (12). Interphase extract containing *Xenopus* sperm nuclei was induced to enter mitosis and immediately pumped into a microfluidic droplet-generating device prior to nuclear envelope breakdown and the onset of spindle assembly. At the same time, a fluorinated oil/surfactant mixture was pumped into the device through a second inlet. These two discrete, immiscible phases merged at a T-shaped junction within the device to produce stable emulsions of extract droplets in a continuous oil phase (Fig. 1, A and C). Changing the T-junction channel dimensions and relative flow rates of the two phases enabled us to tune droplet volume. Droplet shape could be controlled independently by changing the geometry and dimensions of the device's collection region. In this way, we were able to produce three distinct geometries; spheres, flattened discs, and axially elongated “slugs” (Fig. 1, B and C). Following encapsulation, nuclei size and shape resembled that of their unencapsulated counterparts (Fig. 1C), suggesting that the process of droplet-generation did not appreciably perturb nuclear morphology.

To examine the relationship between steady-state spindle length and cytoplasmic volume, interphase nuclei were encapsulated within spherical droplets ranging in diameter from 20–120 μm . Bipolar spindle assembly was observed in droplets of greater than $\sim 30 \mu\text{m}$ diameter, permitting measurements of spindle length using fluorescence microscopy (Fig. 2, A and B). Spindles exhibited isometric scaling, so we used the single metric of spindle length to serve as a reasonable proxy for spindle “size” (Fig. 2A). This also allowed direct comparisons with previously published scaling data in which length was the only reported spindle dimension. These measurements defined two distinct regimes that described the relationship between spindle length and droplet diameter: in droplets with diameters larger than $\sim 80 \mu\text{m}$, spindle length was relatively constant, reaching an upper limit similar to the average spindle length found in unencapsulated extract ($\sim 40.5 \pm 4.4 \mu\text{m}$), whereas in smaller droplets, spindle length scaled almost linearly with droplet diameter (Fig. 2B).

These results shared remarkable similarity with spindle scaling observed during *Xenopus* development, particularly in the linear scaling regime (2) (Fig. 2, C and D). Within their respective scaling regimes, asymptotic growth fits to the in vivo and in vitro data sets were statistically indistinguishable (solid lines in Fig. 2, B to D; fig. S1 and S2), suggesting that our in vitro system recapitulated the scaling observed in vivo. Scaling was observed in droplets ranging in diameter from ~ 30 to $80 \mu\text{m}$, corresponding to cell sizes typical of Stage 8 and Stage 9 of *Xenopus* development (Fig. 2D), a temporal window that encompasses the mid-blastula transition and the onset of zygotic transcription (13, 14). Because *Xenopus* egg

extracts are effectively static in a developmental context, changes in cytoplasmic composition that might affect scaling in the intact embryo do not occur in our system (e.g. (15)). Thus, developmental cues can be eliminated as a potential model for the spindle scaling observed in these droplets, leaving the two remaining hypothetical mechanisms, component limitation and/or boundary sensing.

A boundary sensing mechanism predicts that changing the physical dimensions of the encapsulating droplet, while holding droplet volume constant, should impact spindle length. To test this model, the lengths of spindles assembled in spheres were compared to those assembled in longer, isovolumetric slugs. Employing slugs as opposed to flattened spheres allowed spindle assembly to be restricted in two of three dimensions over a broader aspect ratio range (Fig. 3A). To ensure that encapsulated spindle lengths could vary in response to changes in droplet shape, slugs used in these experiments were generated by geometrically confining spheres ranging in diameter from 40–60 μm (the approximate midpoint of the scaling regime; Movie S2). Differences in spindle lengths for these two extract droplet geometries were statistically indistinguishable (Student's *t*-test, $p = 0.2$ for all slug and sphere data between 40–60 μm). Furthermore, spindle length remained relatively constant despite three-fold increases in slug length over a narrow range of cytoplasmic volumes (Fig. 3, B and C, fig. S3). Collectively, these results opposed the predictions of a boundary sensing model for spindle length regulation and suggested that cytoplasmic shape was not likely a major determinant of spindle length.

Through a variety of different mechanisms, spindles *in vivo* demonstrate a remarkable ability to correctly position themselves near the cell center prior to the onset of anaphase and cytokinesis. (16–20). Each implicitly requires the spindle be able to “sense” its position relative to cellular boundaries. In the absence of boundary sensing, spindle position within a cell (or a confining extract volume) is expected to be random. To test this prediction, we plotted spindle position relative to the volumetric centers of confining spheres and slugs (Fig. 4, A and B). In both geometries, spindles tended to localize toward the droplet center, to a greater extent than expected for uniform random positioning (Fig. 4, A and B; Movies S3). This trend was more pronounced in smaller droplets (Fig. 4, A and B residual plots). In contrast, the positions of encapsulated polystyrene beads aligned more closely with average random positions (Fig. 4, A and B residual plots; figs. S1 and S2 and Movie S4). This suggested that the weak convective flows observed in some slugs were likely not responsible for spindle centering (e.g. see Movie S5). The distribution of spindle orientations relative to the slug long axis was found to be $31 \pm 16^\circ$ (Fig 4C), indicating that, like in cells, a spindle is more likely to align parallel to the long-axis of its enclosure (21), even in the absence of a cortical membrane and associated pulling forces. Indeed, peripheral spindle microtubules extend well beyond the spindle proper, effectively increasing its size (22). Perhaps these peripheral microtubules exert pushing forces against droplet boundaries resulting in centering (23). Alternatively, spindle proximity to a droplet boundary might influence the distribution of forces generated by microtubule-associated motors pulling against the bulk cytoplasm (19, 24). Thus, a boundary sensing mechanism might indeed work to affect spindle position, but contributes little, if at all, to determining spindle length.

Collectively, our data indicate that changes in cytoplasmic volume are sufficient to account for the spindle scaling as it occurs in vivo (2). By eliminating alternative hypothetical models, the data support a scaling mechanism in which a limiting pool of cytoplasmic component(s) regulates spindle length (8, 11). In large droplets or cells, like in unbounded extract, spindle length appears to be constrained by mechanisms intrinsic to the spindle (2, 25). Once cytoplasmic volume is reduced to a critical threshold, components become limited, which produces smaller spindles. This process serves as a passive, yet robust way for cells to control the size of their spindles and possibly other internal structures.

Supplementary Material

Refer to Web version on PubMed Central for supplementary material.

Acknowledgments

We would like to thank T. Salmon and T. Mitchison for their insightful reviews of the manuscript as well as M. Wuhr for his comments on the work and for providing access to raw data originally presented in (2). We also thank L. Edens, C. Geisler, D. Fay and D. Levy in the Molecular Biology Department at the University of Wyoming for their critical review of the manuscript and helpful suggestions. Lastly, the authors would like to express thanks to A. Groen for providing the labeled anti-NuMA antibodies used in these studies. This work was supported by NIH grants R01 GM102428 (to J.C.G.) and R15 GM101636 (to J.O.) and by the NIH-funded Wyoming INBRE program (P20RR016474 and P20GM103432).

References and Notes

1. Montorzi M, Burgos MH, Falchuk KH. *Xenopus laevis* embryo development: arrest of epidermal cell differentiation by the chelating agent 1,10-phenanthroline. *Mol Reprod Dev.* Jan.2000 55:75. [PubMed: 10602276]
2. Wuhr M, et al. Evidence for an upper limit to mitotic spindle length. *Curr Biol.* Aug 26.2008 18:1256. [PubMed: 18718761]
3. Courtois A, Schuh M, Ellenberg J, Hiiragi T. The transition from meiotic to mitotic spindle assembly is gradual during early mammalian development. *J Cell Biol.* Aug 6.2012 198:357. [PubMed: 22851319]
4. Hara Y, Kimura A. Cell-size-dependent spindle elongation in the *Caenorhabditis elegans* early embryo. *Curr Biol.* Sep 29.2009 19:1549. [PubMed: 19682904]
5. Bird SL, Heald R, Weis K. RanGTP and CLASP1 cooperate to position the mitotic spindle. *Mol Biol Cell.* Aug.2013 24:2506. [PubMed: 23783028]
6. Kiyomitsu T, Cheeseman IM. Chromosome- and spindle-pole-derived signals generate an intrinsic code for spindle position and orientation. *Nat Cell Biol.* Mar.2012 14:311. [PubMed: 22327364]
7. Sharp DJ, et al. Functional coordination of three mitotic motors in *Drosophila* embryos. *Mol Biol Cell.* Jan.2000 11:241. [PubMed: 10637305]
8. Decker M, et al. Limiting amounts of centrosome material set centrosome size in *C. elegans* embryos. *Curr Biol.* Aug 9.2011 21:1259. [PubMed: 21802300]
9. Ludington WB, Shi LZ, Zhu Q, Berns MW, Marshall WF. Organelle size equalization by a constitutive process. *Curr Biol.* Nov 20.2012 22:2173. [PubMed: 23084989]
10. Chan YH, Marshall WF. Scaling properties of cell and organelle size. *Organogenesis.* Apr.2010 6:88. [PubMed: 20885855]
11. Goehring NW, Hyman AA. Organelle growth control through limiting pools of cytoplasmic components. *Curr Biol.* May 8.2012 22:R330. [PubMed: 22575475]
12. Desai, A.; Murray, AW.; Mitchison, T.; Walczak, CE. *Methods in Cell Biology.* Vol. 61. Academic Press; 1999. p. 385-412.

13. Newport J, Kirschner M. A Major Developmental Transition in Early *Xenopus*-Embryos. 1. Characterization and Timing of Cellular-Changes at the Midblastula Stage. *Cell*. 1982; 30:675. [PubMed: 6183003]
14. Nieuwkoop, PD.; Faber, J., editors. Normal table of *Xenopus laevis* [Daudin] - a systematical and chronological survey of the development from the fertilized egg till the end of metamorphosis. 2. North-Holland Pub. Co; Amsterdam: 1967.
15. Wilbur JD, Heald R. Mitotic spindle scaling during *Xenopus* development by kif2a and importin alpha. *Elife*. 2013; 2:e00290. [PubMed: 23425906]
16. Gonczy P, Grill S, Stelzer EH, Kirkham M, Hyman AA. Spindle positioning during the asymmetric first cell division of *Caenorhabditis elegans* embryos. *Novartis Found Symp*. 2001; 237:164. [PubMed: 11444042]
17. Lee L, et al. Positioning of the mitotic spindle by a cortical-microtubule capture mechanism. *Science*. Mar 24.2000 287:2260. [PubMed: 10731147]
18. Minc N, Burgess D, Chang F. Influence of cell geometry on division-plane positioning. *Cell*. Feb 4.2011 144:414. [PubMed: 21295701]
19. Mitchison T, et al. Growth, interaction, and positioning of microtubule asters in extremely large vertebrate embryo cells. *Cytoskeleton (Hoboken)*. Oct.2012 69:738. [PubMed: 22786885]
20. Tolic-Norrelykke IM, Sacconi L, Thon G, Pavone FS. Positioning and elongation of the fission yeast spindle by microtubule-based pushing. *Curr Biol*. Jul 13.2004 14:1181. [PubMed: 15242615]
21. Wuhr M, Tan ES, Parker SK, Detrich HW 3rd, Mitchison TJ. A model for cleavage plane determination in early amphibian and fish embryos. *Curr Biol*. Nov 23.2010 20:2040. [PubMed: 21055946]
22. Gatlin JC, et al. Spindle fusion requires dynein-mediated sliding of oppositely oriented microtubules. *Curr Biol*. Feb 24.2009 19:287. [PubMed: 19230671]
23. Holy TE, Dogterom M, Yurke B, Leibler S. Assembly and positioning of microtubule asters in microfabricated chambers. *Proc Natl Acad Sci U S A*. Jun 10.1997 94:6228. [PubMed: 9177199]
24. Wuhr M, Dumont S, Groen AC, Needleman DJ, Mitchison TJ. How does a millimeter-sized cell find its center? *Cell Cycle*. Apr 15.2009 8:1115. [PubMed: 19282671]
25. Dumont S, Mitchison TJ. Force and length in the mitotic spindle. *Curr Biol*. Sep 15.2009 19:R749. [PubMed: 19906577]
26. Maresca TJ, Heald R. Methods for studying spindle assembly and chromosome condensation in *Xenopus* egg extracts. *Methods Mol Biol*. 2006; 322:459. [PubMed: 16739744]
27. Mitchison. vol. 2013.
28. Waterman-Storer, C. *Current Protocols in Cell Biology*. John Wiley & Sons, Inc; 1998. Microtubule/Organelle Motility Assays; p. 13.1.1-13.1.21.
29. Duffy DC, McDonald JC, Schueller OJA, Whitesides GM. Rapid prototyping of microfluidic systems in poly(dimethylsiloxane). *Analytical Chemistry*. Dec 1.1998 70:4974. [PubMed: 21644679]
30. Xia YN, Whitesides GM. Soft lithography. *Angew Chem Int Edit*. Mar 16.1998 37:551.
31. Dendukuri D, Tsoi K, Hatton TA, Doyle PS. Controlled synthesis of nonspherical microparticles using microfluidics. *Langmuir*. Mar 15.2005 21:2113. [PubMed: 15751995]

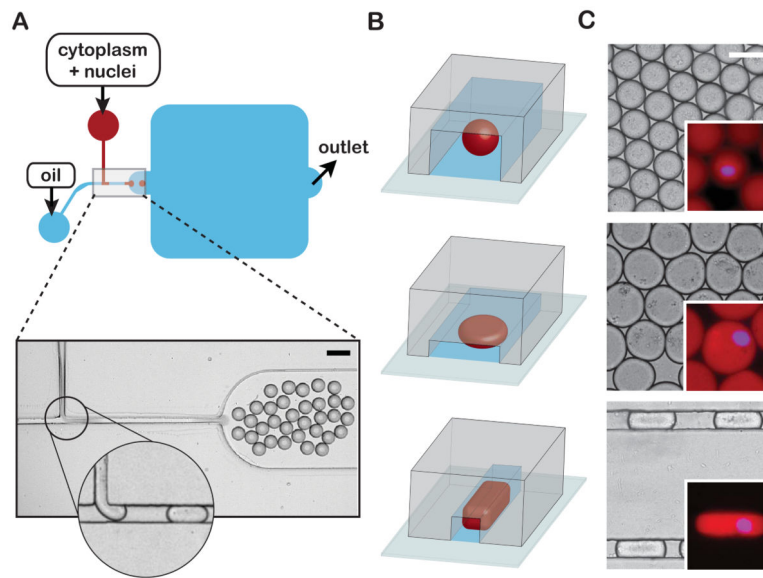


Fig. 1.

Microfluidic encapsulation of nuclei in cytoplasmic volumes of defined size and shape. **(A)** Top panel - Simplified schematic of a PDMS microfluidic device featuring a classic T-junction droplet generator and collection reservoir (blue rounded-square). An extract phase containing nuclei (red) is continuous until sheared off into droplets by the oil/surfactant phase (blue). Bottom panel - a representative image of droplet generation at a standard T-junction. The magnified inset shows a formed droplet moving toward the collection reservoir and another about to be sheared from the extract phase (see Movie S1). Scale bar = 100 μm . **(B)** Alternative droplet shapes result from changing the collection reservoir geometry: spheres (top panel), flattened disks (middle panel) and elongated slug-shaped droplets (bottom panel). **(C)** Representative micrographs of spheres, discs, and slugs contained within reservoirs/channels. Scale bar = 50 μm . Insets: Magnified images of droplets encapsulating “cycled” interphase sperm nuclei. Nuclear DNA was stained with DAPI to access nuclear morphology (blue) and soluble tubulin (pseudo-colored red, labeled with Atto-488) was used to visualize droplet boundaries. All droplets are approximately isovolumetric. Inset scale bar = 50 μm .

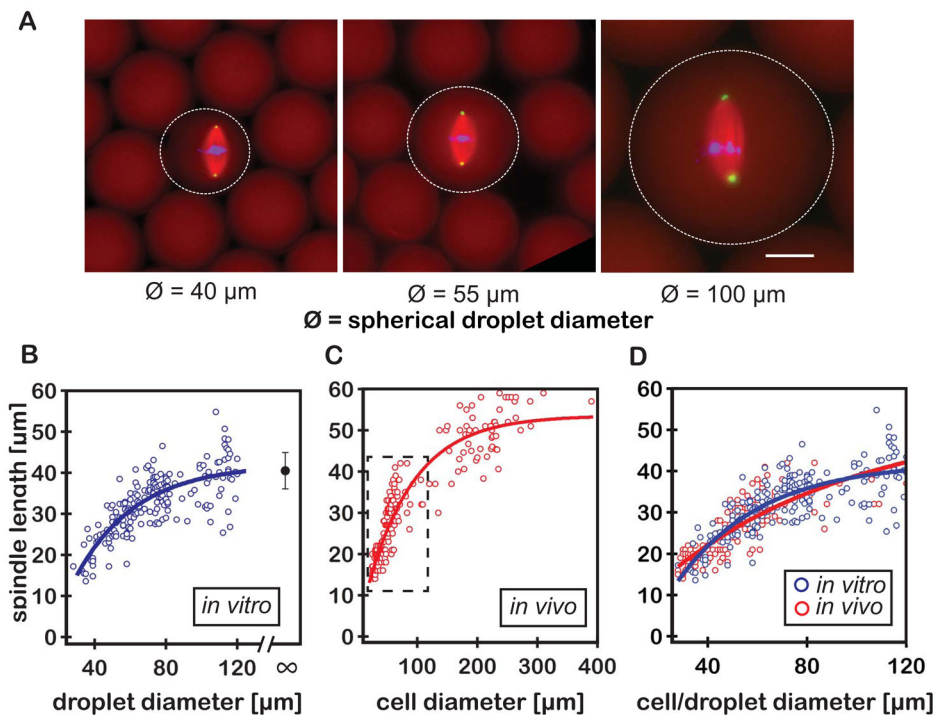


Fig. 2.

Developmental spindle scaling can be recapitulated *in vitro* in the absence of developmental cues or a functional cell cortex. **(A)** Representative fluorescent images of spindles assembled in spherical extract droplets of various sizes. Spindles were labeled by adding fluorophores to the extract prior to droplet formation; tubulin to visualize microtubules (pseudo-colored red, labeled with Atto-488), DAPI to visualize DNA (blue), and directly labeled antibodies against NuMA to visualize spindle poles (pseudo-colored green, Atto-568 α -NuMA). Dashed circles indicate droplet boundaries as visualized by the extent of soluble labeled tubulin. Scale bar = 25 μm . **(B)** Spindle length plotted as a function of encapsulating droplet diameter (blue open circles, $n=96$ spindles). The single black circle indicates the average spindle length in unencapsulated extract (mean \pm SD; $n=81$ spindles). **(C)** Spindle length at metaphase plotted as a function of cell size during early (stage 8 to 9) *Xenopus* embryo development (red open circles, adapted from (2)). **(D)** Comparison of spindle scaling *in vitro* and *in vivo* (blue and red open circles, respectively; with corresponding fits). Each data set was fit using a three-parameter equation that assumes asymptotic growth (solid lines in Fig. 2, B to D; fig. S1 and S2).

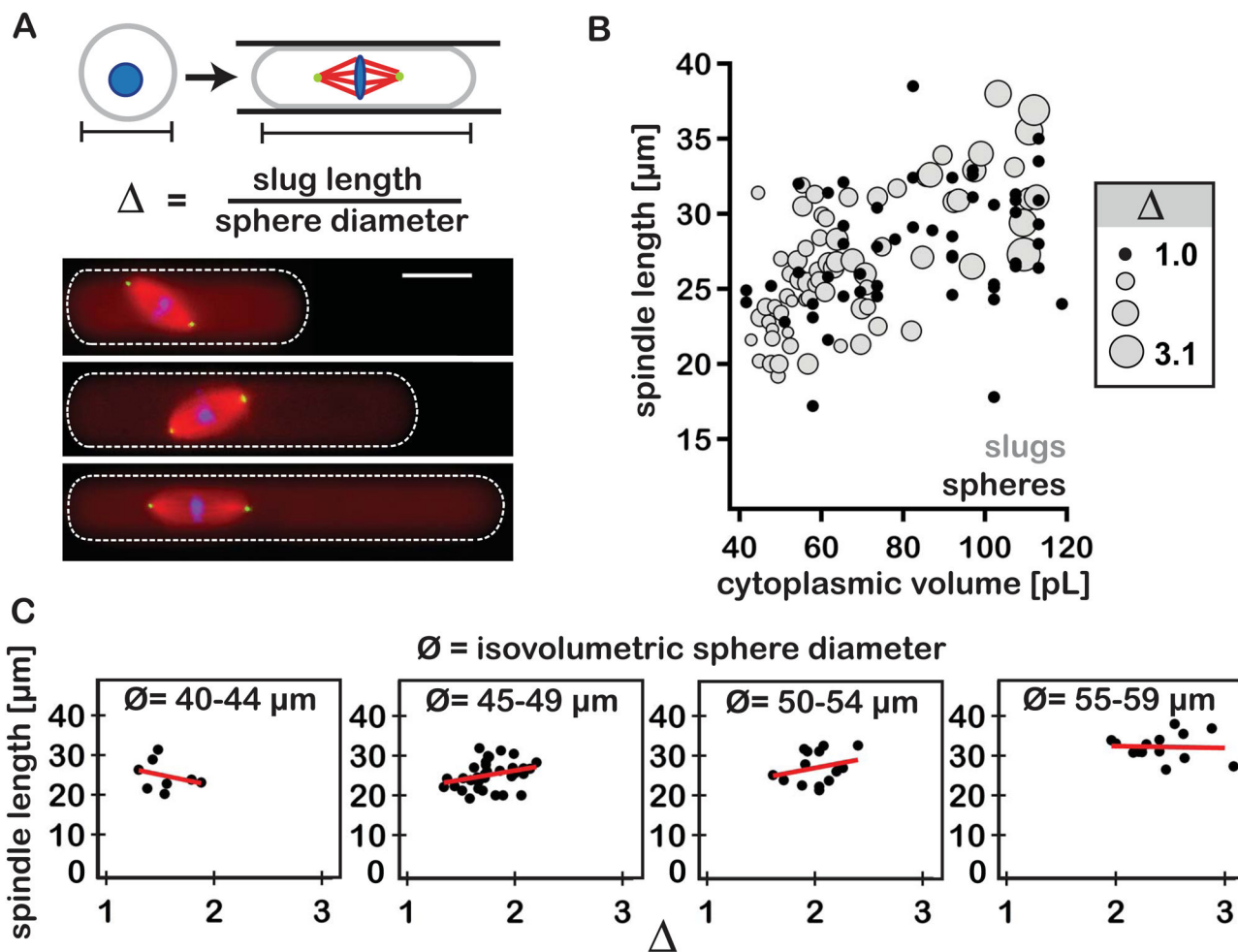


Fig. 3.

Reductions in cytoplasmic volume account for the spindle scaling observed in vitro. (A) Top panel – cartoon depicting the transformation of spherical droplet into an isovolumetric slug, and the calculation of extent of elongation (Δ). Bottom panel – fluorescent images of representative spindles assembled in slugs of increasing Δ . Fluorophores were added to the extract as described in Fig. 2. (B) Graph shows spindle length plotted as a function of droplet cytoplasmic volume. For shaded markers (grey circles, $n=71$ spindles), marker size is proportional to the ratio of slug long axis length over the diameter of an isovolumetric sphere (i.e. extent of elongation, denoted as Δ). Solid markers (black circles) represent data derived from spherical droplets (i.e. $\Delta=1$, $n=96$ spindles). (C) Plots of spindle length as a function of extent of elongation under near-isovolumetric conditions (i.e. binned by isovolumetric sphere diameter, \emptyset). Linear trend lines (red) exhibit variable slopes indicating a lack of a constant relationship between the two measurements.

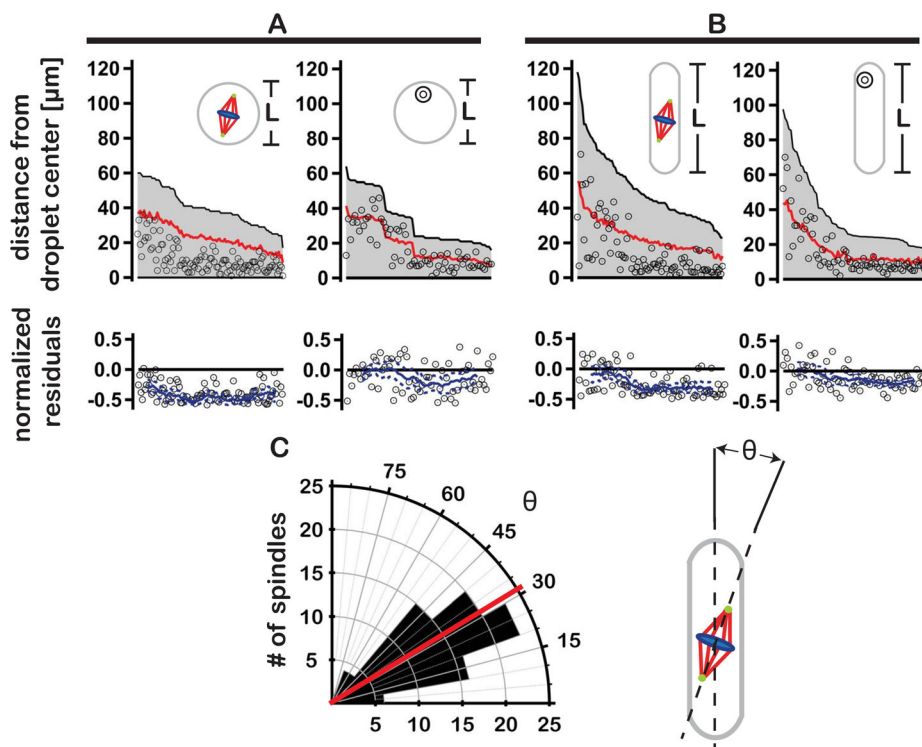


Fig. 4.

Spindles exhibit non-random positioning in spheres and slugs. **(A)** Plots show the positions of spindles (left panel) and polystyrene beads (right panel) within spherical droplets. Black lines in each of the plots reflect the distance between the droplet center and its most distal edge ($L/2$, shown schematically in insets). Open circles indicate the positions of spindles/beads in relation to the droplet center. Red lines depict the average absolute displacement of spindles/beads expected for uniform random positioning (see supplementary material). Corresponding residual plots show the normalized difference between the center-to-center position of the spindle or bead and the theoretical random position. Solid blue lines represent the moving average of residual values (with upper and lower 95% confidence intervals indicated by dashed blue lines). **(B)** As in A, spindle and bead positions in axially elongated slugs. **(C)** Spindle orientation in slugs. Left panel - polar histogram plot showing the angle θ between the inter-polar spindle axis and the long axis of the confining slug (red line indicates the average orientation angle; $n = 89$ spindles). Right panel – cartoon depicting the determination of angle θ .